

Rate Constants for $\text{H} + \text{O}_2 + \text{M}$ at 298 K for $\text{M} = \text{He}, \text{N}_2,$ and H_2O

K.-J. Hsu, J. L. Durant,* and F. Kaufman†

Department of Chemistry, University of Pittsburgh, Pittsburgh, Pennsylvania 15260

(Received: August 28, 1986)

The rate constants of the three-body recombination reaction $\text{H} + \text{O}_2 + \text{M}$ ($\text{M} = \text{He}, \text{N}_2, \text{H}_2\text{O}$) were measured from 4.79 to 30.1 Torr at room temperature by the discharge-flow technique. The respective rate constants obtained are $(2.6 \pm 0.2) \times 10^{-32}$, $(6.1 \pm 0.9) \times 10^{-32}$, and $(6.4 \pm 0.8) \times 10^{-31} \text{ cm}^6 \text{ s}^{-1}$. Although the rates for He and N_2 can be rationalized in terms of existing theory, that for H_2O implies a collision efficiency greater than 1. This situation can be rectified by use of the total quantum mechanical scattering cross section instead of the Lennard-Jones cross section commonly used.

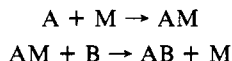
Introduction

The study of recombination reactions in the gas phase has a practical, direct payoff in the measurement of rate constants and also provides a test for theoretical predictions concerning chemical interactions and energy-transfer processes. The recombination of H with O_2 is important in reactive systems as diverse as combustion and upper atmospheric chemistry. Because of the relative stability of HO_2 the recombination may be viewed as a chain-terminating reaction.¹ The competition between hydroperoxy radical formation and the chain-branching reaction $\text{H} + \text{O}_2 \rightarrow \text{OH} + \text{O}$ helps fix the location of the $\text{H}_2\text{-O}_2$ second explosion limit.² The recombination reaction also contributes significantly to both the energy release and the O_2 consumption rates in hydrogen flames.³ In the atmosphere, the recombination reaction is responsible for the efficient conversion of free H to HO_2 .⁴

The $\text{H} + \text{O}_2 + \text{M}$ reaction has been extensively studied for a variety of bath gases, M. A comprehensive review of older work can be found in Baulch et al.'s evaluation,⁵ with more recent results reviewed by Warnatz,¹ as well as in the CODATA and NASA/JPL evaluations.^{6,7} Room temperature experiments⁸ show that the recombination is in the limiting third-order region at pressures below a few atmospheres even for relatively efficient third bodies such as CH_4 . It was also estimated⁸ that an approach to within 20% of the high-pressure limit rate k_∞ would require pressures on the order of 2000 atm.

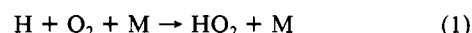
There have been a wide variety of calculations performed on the $\text{H} + \text{O}_2 + \text{M}$ system. Melius and Blint have produced a full analytic potential surface,⁹ while other groups have focussed on the $\text{H} + \text{O}_2$ reaction coordinate. These latter studies suggest that the barrier to reaction is small¹⁰ or nonexistent,¹¹ instead of the 2.3 kcal/mol barrier proposed by Melius and Blint. The Melius-Blint surface has been used in a wide range of trajectory calculations on HO_2 dissociation¹² and collisional energy transfer,^{13,14} with an eye toward calculating recombination rates.^{14,15}

Theoreticians have applied a variety of methods to calculate rates for recombination, $\text{A} + \text{B} + \text{M} \rightarrow \text{AB} + \text{M}$. Perhaps the most widely used is due to Troe.¹⁶ His method is based on an approximate analytical solution of the master equation appropriate for AB formation, followed by collisional stabilization by M. Multiplicative correction factors are then included to mitigate the effects of the initial approximations. An alternate approach, taken by Keck and co-workers,^{17,18} has achieved some success in modeling atom recombination reactions. They adopt a phase space formalism and calculate the flux through a surface dividing the separated reactants from the recombined products. This flux is then corrected for recrossing effects by using results from a more detailed trajectory study. This approach implicitly treats both the microscopic reaction scheme, considered by Troe, and the chaperone mechanism, involving AM or BM intermediates, e.g.



A theme common to these treatments is the influence of the potential energy surface on the reactions.^{18,19} Indeed, Shui and Appleton²⁰ suggest that the study of recombination reactions could yield as much data about the long-range attractive part of the potential surface as molecular beam scattering does about the repulsive part of the potential.

We have undertaken a comprehensive study of the recombination reaction



with the goal of producing a body of self-consistent data for a number of bath gases, spanning the pressure range from 4 to 70 Torr and the temperature range from 298 to 1000 K. A new flow tube apparatus with a differentially pumped detection cell, fitted for resonance fluorescence detection of H, OH, and HO_2 (by chemical titration), was designed and constructed for this purpose. In this, the first report on this work, we will concentrate on the experimental technique and the results obtained at room temperature with the bath gases He, N_2 , and H_2O .

Experimental Section

The flow reactor used in this work is shown schematically in Figure 1. The major difference between this apparatus and other discharge flow systems is the use of a differentially pumped optical detection cell. The pressure drop occurring at the sampling orifice effectively stops the termolecular reaction, a feature important for studies at elevated temperatures. The pressure drop also serves to reduce collisional quenching of the resonance fluorescence signal. It should be noted that the pressure in the detection cell was high

(1) Warnatz, J. In *Combustion Chemistry*, Gardiner, Jr., W. C., Ed.; Springer-Verlag: New York, 1984; p 197.

(2) Dixon-Lewis, G.; Williams, D. J. "Oxidation of Hydrogen and Carbon Monoxide" In *Comprehensive Chemical Kinetics*, Vol. 17, Bamford, C. H., Tipper, C. F. H., Ed.; Elsevier: Amsterdam, 1977.

(3) Miller, J. A.; Kee, R. J. *J. Phys. Chem.* 1977, 81, 2534.

(4) Brasseur, G.; Solomon, S. *Aeronomy of the Middle Atmosphere: Chemistry and Physics of the Stratosphere and Mesosphere*, Reidel: Boston, 1984.

(5) Baulch, D. L.; Drysdale, D. D.; Horne, D. G.; Lloyd, A. C. *Evaluated Kinetic Data for High Temperature Reactions*, Vol. 1; CRC: Cleveland, 1972.

(6) Baulch, D. L.; Cox, R. A.; Hampson, R. F.; Kerr, J. A.; Troe, J.; Watson, R. T. *J. Phys. Chem. Ref. Data* 1984, 13, 1259.

(7) DeMore, W. B., et al. "Chemical Kinetics and Photochemical Data for Use in Stratospheric Modeling," Evaluation 7, NASA/JPL, Pasadena, CA, 1985.

(8) Cobos, C. J.; Hippler, H.; Troe, J. *J. Phys. Chem.* 1985, 89, 342.

(9) Melius, C. F.; Blint, R. *J. Chem. Phys. Lett.* 1979, 64, 183.

(10) Dunning, T. H.; Walch, S. P.; Goodgame, M. M. *J. Chem. Phys.* 1981, 74, 3482.

(11) Langhoff, S. R.; Jaffe, R. L. *J. Chem. Phys.* 1979, 71, 1475.

(12) Miller, J. A.; Brown, N. J. *J. Phys. Chem.* 1982, 86, 772.

(13) Miller, J. A.; Brown, N. J. *J. Chem. Phys.* 1984, 80, 5568.

(14) Gallucci, L. G.; Schatz, G. C. *J. Phys. Chem.* 1982, 86, 2352.

(15) Blint, R. J. *J. Chem. Phys.* 1980, 73, 765.

(16) Troe, J. *J. Phys. Chem.* 1979, 83, 114.

(17) Shiu, V. H.; Appleton, J. P.; Keck, J. C. *J. Chem. Phys.* 1970, 53, 2547.

(18) Shiu, V. H.; Appleton, J. P.; Keck, J. C. *Symp. (Int.) Combust. [Proc.]*, 13th, 1971, 19.

(19) Cobos, C. J. *Int. J. Chem. Kinet.* 1986, 18, 459.

(20) Shui, V. H.; Appleton, J. P. *J. Chem. Phys.* 1971, 55, 3126.

* Present address: Combustion Research Facility, Div. 8353, Sandia National Laboratories, Livermore, CA 94550.

† Deceased July 6, 1985.

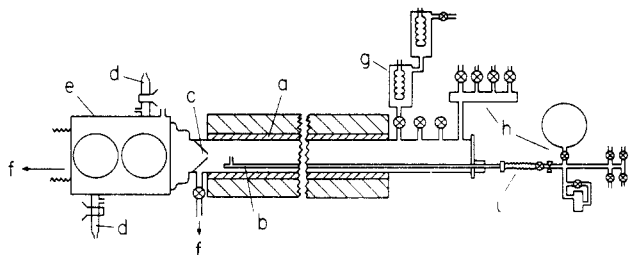


Figure 1. Experimental apparatus: (a) flow tube; (b) moveable injector; (c) sampling orifice; (d) resonance fluorescence lamps; (e) detection cell; (f) pumps; (g) thermal dissociator; (n) stable reagent inlet; (i) flexible hose.

enough (0.25–1 Torr) to prevent molecular beam formation.

The sampling orifice ($d \sim 3.5$ mm) was located at the apex of a quartz cone centered on the downstream end of the flow tube. The detection cell was pumped by a Roots blower (30 L/s at 1 Torr). An adjustable air bleed downstream of the cell was used to slow the effective pumping speed of the Roots blower, allowing the pressure drop across the orifice to be varied from a factor of 20 to 90. The detection cell was constructed from a 4-in. o.d., 5-in. long aluminum cylinder, with a 5-cm i.d. hole bored through it. The inside surfaces of the cell were Teflon coated to reduce wall losses of atoms and radicals. Two detection regions were formed by the intersection of two pairs of orthogonal ports. Wood's horns were mounted opposite the resonance lamps and detectors to reduce scattered light. Flow velocities in the detection cell were approximately 1500 cm/s.

Atomic hydrogen was monitored in the first detection region, located 10 cm downstream from the sampling orifice. The resonance lamp was of standard design,²¹ utilizing a slow flow of He at approximately 1 Torr pressure and a microwave discharge (Raytheon Microtherm, 2450 Mhz, 20-W forward power) for excitation. A MgF_2 window, baffles, and vacuum UV monochromator (ARC VW 502) orthogonal to the lamp excitation collected and filtered the Lyman α resonance fluorescence signal, which was then detected by a solar blind photomultiplier tube (EMR 541 G). The photomultiplier signal was conditioned with a pulse amplifier/discriminator (E.G. & G. 1182) and counted (Tennelec TC 535P). The counter output was buffered (Tennelec TC 588) and directed to a computer (HP 9121) for further analysis. The typical detection limit for H in this system ($S/N = 1$) corresponded to $[\text{H}] = 2 \times 10^9 \text{ cm}^{-3}$ in the detection cell. Typical initial count rates were about 500 counts in a 10-s integration period.

The second detection region, located 15 cm from the orifice, was used for OH detection. The lamp was similar to that used for H atoms, but operated at 2 Torr, with $\sim 20\%$ of the He flow diverted through a water bubbler before entering the lamp. The resonance fluorescence was collected at right angles to the excitation and passed through a filter to isolate the $\text{OH}(A \rightarrow X)$ transition (310 nm, fwhm bandpass of 12.5 nm). The filtered resonance fluorescence was detected by an EMI 9789QA photomultiplier. The remaining signal processing paralleled that for H atoms. The typical detection limit was $[\text{OH}] = (2-3) \times 10^9 \text{ cm}^{-3}$ in the detection cell. Typical count rates ranged up to 700 counts in a 10-s integration period. Absolute $[\text{OH}]$ was determined by addition of a small, known $[\text{NO}_2]$ through the injector to excess $[\text{H}]$ and measuring the resulting OH signal. H-atom detection could then be calibrated by addition of excess $[\text{NO}_2]$ to the unknown $[\text{H}]$ and measuring the resulting OH signal. HO_2 was monitored by conversion to OH via reaction with excess NO introduced into the detection cell 7-cm upstream of the OH detection port. To ensure thorough mixing, the NO was added through a 1-cm-long capillary tube.

The flow tube was constructed of 2.54-cm i.d. quartz tube and was 110 cm long. It was pumped by a 5 L/s mechanical pump (Welch 1397) producing flow velocities in the main tube between

900 and 1200 cm/s. The reaction zone was limited to the last 55 cm in order to provide sufficient length for development of the laminar profile. A 7-mm o.d. moveable quartz injector located on the bottom of the flow tube was used to add molecular oxygen. The flow tube and injector were coated with halocarbon wax to reduce the surface loss rates, to typical rates of $k_{w,\text{OH}} = 10-20 \text{ s}^{-1}$ and $k_{w,\text{H}} < 2 \text{ s}^{-1}$.

Wall loss rates for H and OH were measured directly by using moveable radical sources. For H, hydrogen atoms from a microwave discharge were introduced into the flow tube by the moveable injector. In order to measure the OH wall loss, a known amount of NO_2 , with $[\text{NO}_2] < [\text{H}]_0$, was introduced through the injector to produce OH via $\text{H} + \text{NO}_2 \rightarrow \text{OH} + \text{NO}$. $[\text{H}]$ was sufficiently large to drive the reaction to completion. Moving the injector thus changed the point of OH production, allowing the wall loss to be ascertained.

For kinetic experiments the hydrogen atom source was fixed and consisted of either a thermal dissociator or a microwave discharge. $[\text{H}]$ ranged from 1×10^{12} to $5 \times 10^{12} \text{ cm}^{-3}$. For the bulk of this study, a dissociator based on Trainor's design²² was used. In this design a hydrogen/helium mixture was passed over a resistively heated tungsten filament. The advantage of this method is its selective production of H atoms, though it suffers from a dissociation yield of only 1–2%. The microwave discharge, on the other hand, boasts yields of up to 50%, allowing much lower $[\text{H}_2]$ to be used. This reduces some complications due to secondary chemistry, especially at higher temperatures. A drawback to the method is the nonselective nature of radical production. He flowing to the microwave discharge was passed through a 900 K copper oven and a liquid nitrogen cooled molecular sieve trap to lower $[\text{O}]$ and $[\text{OH}]$ to acceptable levels. The measured rate constants were independent of the method of H atom generation.

Pressures in the system were measured with stainless steel transducers (Validyne, Model DP7 with ranges of ± 0.1 and 1 psi) calibrated against oil manometers. Flow rates for gases were measured by using five Tylan mass flowmeters (Tylan Models FM360 and FM361) which were calibrated by using a Hg sealed piston gauge (Brooks Vol-U-Meter). Water was taken from a reservoir heated to $\sim 70^\circ \text{C}$. Its flow rate was measured by the timed pressure rise in a bulb of known volume. The variation in H_2O flow measured this way was always less than 8% over the course of a day.

He carrier gas (Air Products or Matheson UHP 99.999%) was passed through a molecular sieve trap held at 77 K before entering the dissociator or flow tube. Hydrogen (Matheson, Matheson Grade 99.9995% or Matheson 1% H_2 in He) was purified by passage over a heated tungsten filament, followed by a 77 K trap. O_2 (Matheson, UHP 99.99%) and N_2 (Matheson, Prepurified 99.998%) were used without further purification.

Data Analysis

The experimentally observed pseudo-first-order rate constants, k_{obsd}^1 , were measured by recording the $[\text{H}]$ resonance fluorescence signal as a function of the O_2 injector position under conditions of excess O_2 , with $50 < [\text{O}_2]/[\text{H}]_0 < 300$ (Figure 2). Five to ten decays were taken with $[\text{O}_2]$ chosen so that the pseudo-first-order rates ranged between 10 and 110 s^{-1} . The k_{obsd}^1 were then corrected for an injector effect²³ ranging from 0 to -4 s^{-1} , as measured in each experiment. This injector effect is caused by loss of H atoms on the outside of the injector. As the injector is pulled back, less wall is exposed, and the H atom signal increases (see Figure 2).

We next corrected the k_{obsd}^1 for transport effects. In the pressure range covered by the present study the commonly used plug flow approximation can begin to break down. As the diffusion constant becomes smaller, radial diffusion ceases to be fast enough to remove concentration gradients caused by the parabolic velocity

(22) Trainor, D. W.; Ham, D. O.; Kaufman, F. *J. Chem. Phys.* **1973**, *58*, 4599.

(23) Sridharan, U. C.; Reimann, B.; Kaufman, F. *J. Chem. Phys.* **1980**, *73*, 1286.

(21) Chang, J. S.; Kaufman, F. *J. Chem. Phys.* **1977**, *66*, 4989.

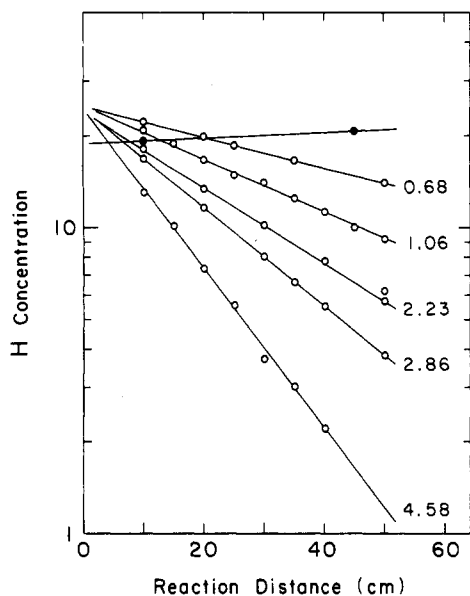


Figure 2. Pseudo-first-order decays; $P_{\text{TOTAL}} = 5.3$ Torr, $P_{\text{N}_2}/P_{\text{TOTAL}} = 0.592$. Filled circles: no O₂ added; open circles: [O₂] (10^{15} cm⁻³) indicated next to each decay. The differing y intercepts are due to drifts in the H atom thermal dissociator efficiency. Direct measurement of wall losses show them to be stable and reproducible.

profile. The axial and radial coordinates become coupled, precluding simple solution of the continuity equation and subsequent evaluation of the effective first-order rate constant.²⁴ The solution of the continuity equation was found, in terms of a power series expansion, by Walker.²⁵ His numerical results were extended by Brown,²⁶ who presented graphs of the solution for commonly encountered input parameters. These permit direct calculation of k^I based on the observed first-order rate and knowledge of the flow velocity, diffusion constant, and wall loss rate. These k^I 's were then compared with those derived by using the plug flow assumption.²⁴

$$k^I = k_{\text{obsd}}^I (1 + k_{\text{obsd}}^I D_{\text{eff}} / v^2)$$

In this treatment the diffusion constants²⁷⁻²⁹ were replaced by effective diffusion coefficients defined by

$$D_{\text{eff}} = D + r^2 v^2 / (48D)$$

where r is the flow tube radius, and v is the mean flow velocity. This equation, which accounts for mass transport by convection as well as diffusion, was derived by Taylor³⁰ and experimentally verified by Plumb, Ryan, and Barton.³¹ The k^I 's derived by these two methods were found to differ by less than 0.1%, validating the use of the plug flow approximation. The axial diffusion corrections applied to k_{obsd}^I to obtain k_{cor}^I were always found to be less than 10% in this work.

In principle, the third-order rate constant could then be obtained by first plotting k_{cor}^I vs. [O₂] at each [M]; the slope k^{II} would be obtained from the slope of each of the resulting lines. Plotting these resulting k^{II} 's vs. [M] would then yield the third-order rate constant. However, life is seldom so simple. Because of the pressure drop across our sampling orifice, our detection limit of

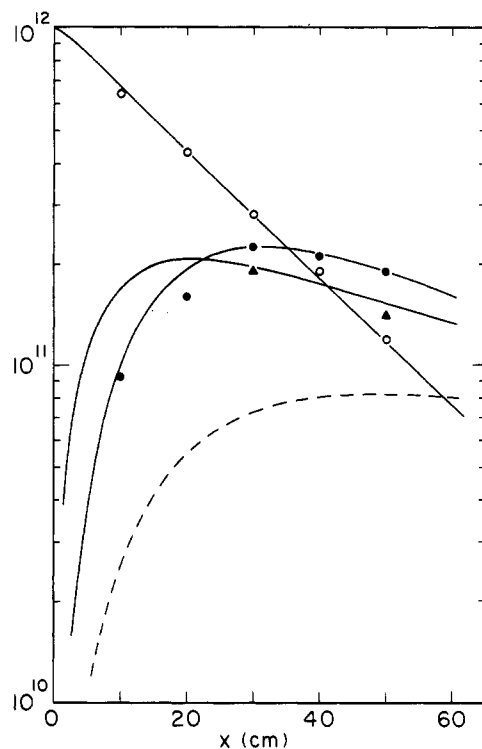


Figure 3. Species concentrations vs. distance; pressure = 13.6 Torr; [O₂] = 2.52×10^{15} cm⁻³; $v = 981$ cm/s; [H], O; [HO₂], ●; [OH], ▲; solid lines are from model calculation, dotted line is $10 \times [\text{O}]$ from calculation.

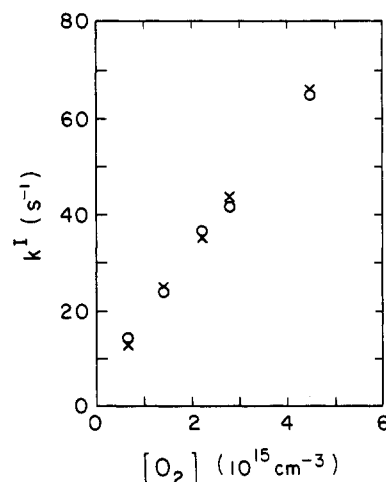


Figure 4. k^I vs. [O₂]: X, observed; O₂ calculated. Note that the slope does not yield k^{II} directly (see text); conditions as in Figure 2.

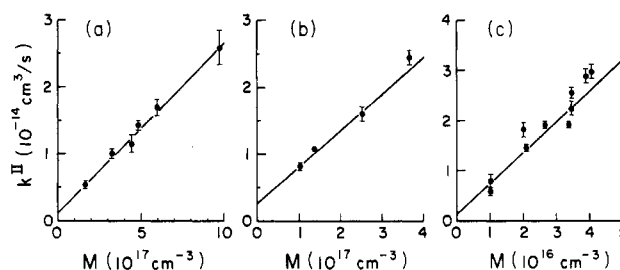


Figure 5. Termolecular plots, k^{II} vs. M . (a) $k^{III}(\text{He}) = (2.6 \pm 0.2) \times 10^{-32}$, (b) $k^{III}(\text{N}_2) = (6.1 \pm 0.9) \times 10^{-32}$, and (c) $k^{III}(\text{H}_2\text{O}) = (6.4 \pm 0.8) \times 10^{-31}$ cm⁶ s⁻¹.

[H] = 2×10^9 cm⁻³ in the detection cell corresponded to detection limits in the flow tube of [H] = $(4-18) \times 10^{10}$ cm⁻³. This necessitated the use of relatively large [H] and required us to consider the effects of secondary chemistry. To do this, we modeled the overall reaction using the first ten reactions listed in Table I. A standard nonlinear differential equation solving algorithm³² was

(24) Kaufman, F. In *Progress in Reaction Kinetics*, Vol. 1, Porter, G., Ed.; Pergamon: New York, 1961; p 1.

(25) Brown, R. L. *J. Res. Natl. Bur. Stand.* **1978**, *83*, 1.

(26) Walker, R. E. *Phys. Fluids* **1961**, *4*, 1211.

(27) Khouw, B.; Morgan, J. E.; Schiff, H. I. *J. Chem. Phys.* **1969**, *50*, 66.

(28) Clifford, A. A.; Mason, R. S.; Waddicor, J. I.; Grey, P. *Proc. R. Soc. London, Ser. A* **1982**, *A380*, 241.

(29) Hirschfelder, J. O.; Curtiss, C. R.; Bird, R. B. *Molecular Theory of Gases and Liquids*; Wiley: New York, 1954.

(30) Taylor, G. *Proc. R. Soc. London, Ser. A* **1953**, *A219*, 186. **1954**, *A225*, 473.

(31) Plumb, I. C.; Ryan, K. R.; Barton, N. G. *Int. J. Chem. Kinet.* **1983**, *15*, 1081.

TABLE I: Reaction Mechanism

	rate, cm ³ /s	sensitivity, %	ref
(1) H + O ₂ + M → HO ₂ + M			
(2) H + HO ₂ → 2OH (87 ± 4%)	7.5 × 10 ⁻¹¹ ^a	-3	35
→ H ₂ O + O (4 ± 2%)			
→ H ₂ + O ₂ (9 ± 4%)			
(3) OH + HO ₂ → H ₂ O + O ₂	7.0 × 10 ⁻¹¹	+1.9	55
(4) OH + OH → H ₂ O + O	1.8 × 10 ⁻¹²	+1.9	6
(5) O + OH → H + O ₂	3.3 × 10 ⁻¹¹	+0.7	56
(6) O + HO ₂ → OH + O ₂	5.4 × 10 ⁻¹¹	-0.7	35
(7) OH $\xrightarrow{\text{wall}}$	25 s ⁻¹	-2.3	
(8) HO ₂ $\xrightarrow{\text{wall}}$	20 s ⁻¹	+0.9	
(9) H $\xrightarrow{\text{wall}}$	2 s ⁻¹	-1.75	
(10) H ₂ + OH → H + H ₂ O	6.1 × 10 ⁻¹⁵	+0.04	57
(11) HO ₂ + HO ₂ → H ₂ O ₂ + O ₂	1.5 × 10 ⁻¹²	not used	58

^a Keyser (ref 36) reports $k_2 = (8.7 \pm 1.5) \times 10^{-11} \text{ cm}^3 \text{ molecule}^{-1} \text{ s}^{-1}$ with branching fractions of $0.9 \pm 0.04:0.02 \pm 0.02:0.08 \pm 0.04$.

used to calculate species concentrations as a function of time (Figure 3). These concentration vs. time profiles were then used to produce a pseudo-first-order decay rate k_{calcd}^I for each O₂ concentration. The least-squares error, Δ , between calculated and observed decay rates was calculated at each pressure by using

$$\Delta^2 = \sum (k_{\text{cor},i}^I - k_{\text{calcd},i}^I)^2 / (k_{\text{cor},i}^I)^2$$

The error was minimized manually by varying $k^{\text{II}} = k^{\text{III}}[\text{M}]$ in steps of $5 \times 10^{-16} \text{ cm}^3 \text{ s}^{-1}$, corresponding to steps of approximately 5% of k^{II} . A representative example of observed and calculated k^{I} 's is shown in Figure 4. Five to ten k^{I} 's were used in determining each k^{II} . The optimized k^{III} values were then plotted vs. $[\text{M}]$ to yield k^{III} (Figure 5). The k^{III} 's thus obtained were 10–50% lower than those obtained by neglecting secondary chemistry. Inclusion of the HO₂ self-reaction was found to be unimportant, changing the derived k^{II} about 0.2%.

To ensure that the model did reproduce the experimental observations, $[\text{H}]$, $[\text{OH}]$, and $[\text{HO}_2]$ were monitored in a series of experiments. The observed concentrations were in very good agreement with those derived from the model, with the average deviation being estimated to be <5% (Figure 3).

The model's sensitivity to variations in input rate constants was tested in a set of calculations for typical experimental conditions: $[\text{H}] = 2 \times 10^{12} \text{ cm}^{-3}$, $[\text{O}_2] = 2 \times 10^{15} \text{ cm}^{-3}$, and $k^{\text{II}} = 1.8 \times 10^{-14} \text{ cm}^3/\text{s}$. For each calculation one rate constant was increased by a factor of 2, resulting in a change in the pseudo-first-order rate k_{calcd}^I . The resulting percent change in the derived k^{III} can be found in Table I. It is gratifying to see that the derived rate constant is nearly independent of these changes in the input rate constants. The most important reaction was found to be H + HO₂, though a doubling of its rate constant produced only a 3.3% change in the derived k^{III} . The accepted uncertainty in k_2 is 60%, while the other reaction rates have uncertainties of 20–30%.⁷ We therefore feel confident that our data analysis faithfully extracts recombination rate constants from our observed decays.

The observed insensitivity of the model results to the input rate constant can be understood if we note that at steady state the relationship between k_1 and k_{obsd} , the observed decay rate, is independent of all of the rate constants, k_2 – k_{11} , and depends only slightly on the branching fraction $x = k_{2c}/(k_{2a} + k_{2b})$. Specifically,³⁴ $k_{\text{obsd}} = 2k_1(3x + 2)/(3x + 3)$, yielding $k_{\text{obsd}} = 1.39k_1$ ($x = 0.1$) or $k_{\text{obsd}} = 1.44k_1$ ($x = 2x$). Thus, we see that the only apparent effect of changing k_2 – k_{11} is altering how near (or far) we are from steady state, which is only weakly reflected in the model rate constants.

Measurements for M = N₂ and H₂O were carried out by using dilutions in He, with $0.27 \leq X_{\text{N}_2} \leq 0.74$ and $0.049 \leq X_{\text{H}_2\text{O}} \leq 0.26$. Data analysis paralleled that for He, with the derived second-order

TABLE II: Selected Rate Constants for H + O₂ + M → HO₂ + M at Room Temperature

reported rate, ×10 ⁻³² cm ⁶ s ⁻¹	method ^a	ref	corrected rate, ×10 ⁻³² cm ⁶ s ⁻¹
M = He, Ar			
2.2 ± 0.2 (He)	DF ^b	33	2.4 ± 0.2
0.75 ± 0.03 (He)	FP ^b	38	2.9 ± 0.7
0.60 ± 0.04 (Ar)	FP ^b	38	2.3 ± 0.6
1.6 ± 0.2 (Ar)	PR	39	
1.6 ± 0.2 (He,Ar)	FP	41	
2.0 ± 0.2 (Ar)	FP	40	
1.9 ± 0.2 (He)	FP	40	
1.9 ± 0.3 (Ar)	DF ^b	34	2.4 ± 0.3
2.5 ± 0.3 (He)	DF ^b	37	
2.8 ± 0.4 (Ar)	FP ^b	8	
2.6 ± 0.2 (He)	DF ^b	this work	
2.5 ± 0.1		average	
M = N ₂			
5.3 ± 0.8	FP	41	
5.5 ± 0.7	FP	40	
6.5 ± 1.0	FP ^b	8	
6.1 ± 0.8	DF ^a	this work	
6.3 ± 0.5		average	
M = H ₂ O			
52 ± 23	DF ^b	33	58 ± 23
64 ± 8	DF ^b	this work	
63 ± 8		average	

^a DF, discharge flow; FP, flash photolysis; PR, pulsed radiolysis.
^b Values used in suggested rate.

rate, k^{II} , being corrected for reaction with He by subtracting $k_{\text{He}}^{\text{III}}[\text{He}]$.

Results and Discussion

The rate constants from this work, together with selected previous rate constants, are presented in Table II. Since the rate constants for Ar and He at room temperature are approximately equal we have listed them together for convenience. We obtained rate constants of $(2.6 \pm 0.2) \times 10^{-32}$ (M = He), $(6.0 \pm 0.9) \times 10^{-32}$ (M = N₂), and $(6.4 \pm 0.8) \times 10^{-31} \text{ cm}^6 \text{ s}^{-1}$ (M = H₂O).

Previous determinations of the H + O₂ + M reaction rate constant have been complicated by uncertainties concerning the secondary reactions. The flow tube studies of Clyne and Thrush³³ and Westenberg and deHaas³⁴ were carried out under conditions where HO₂ was consumed by reaction with H atoms. Steady-state analysis of the resulting kinetic scheme then lead to an expression relating the true rate constant to that observed

$$k_{\text{true}} = 2k_{\text{obsd}}(3x + 2)/(3x + 3)$$

where x is the ratio $k_{2c}/(k_{2a} + k_{2b})$, representing the ratio of chain termination to other channels in the H + HO₂ reaction. They were forced to measure this branching fraction indirectly, obtaining ratios ranging from 0.53³³ to 1.6.³⁴ Using the results of a direct measurement of the branching fraction,^{35,36} we obtain $x = 0.1$. Use of this value allows us to reanalyze the earlier flow tube results, obtaining $k_{1,\text{Ar}} = 2.4 \times 10^{-32} \text{ cm}^6 \text{ s}^{-1}$ for both studies. This value is in good agreement with our value of $(2.6 \pm 0.2) \times 10^{-32}$ and with recent determinations by Hack et al.,³⁷ who measured $(2.5 \pm 0.3) \times 10^{-32}$, and Cobos et al.,⁸ who obtained $(2.8 \pm 0.4) \times 10^{-32}$. The same correction applied to Clyne and Thrush's value for $k_{1,\text{H}_2\text{O}}$ brings their value up to $k = (5.8 \pm 2.3) \times 10^{-31}$, again in good agreement with our value of $(6.4 \pm 0.8) \times 10^{-31} \text{ cm}^6 \text{ s}^{-1}$.

Ahumada, Michael, and Osborne³⁸ studied the recombination reaction by using mercury-sensitized production of H atoms in an H₂/O₂/bath gas mixture. They incorrectly estimated an upper bound for H + HO₂, $k_2 < 10^{-11} \text{ cm}^3 \text{ s}^{-1}$, and concluded that

(35) Sridharan, U. C.; Qiu, L. X.; Kaufman, F. *J. Phys. Chem.* **1982**, *86*, 4569.

(36) Keyser, L. F. *J. Phys. Chem.* **1986**, *90*, 2994.

(37) Hack, W.; Gg. Wagner, H.; Hoyermann, K. *Ber. Bunsen-Ges. Phys. Chem.* **1978**, *82*, 713.

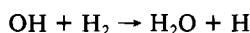
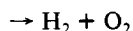
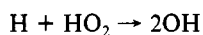
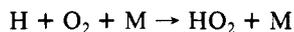
(38) Ahumada, J. J.; Michael, J. V.; Osborne, D. T. *J. Chem. Phys.* **1972**, *57*, 3736.

(32) The program used was adopted from the LSODE mathematics sub-routine package (Painter and Hindmarsh, Lawrence Livermore Laboratory).

(33) Clyne, M. A. A.; Thrush, B. A. *Proc. R. Soc. London, Ser. A* **1963**, *A275*, 559.

(34) Westenberg, A. A.; deHaas, N. *J. Phys. Chem.* **1972**, *76*, 1586.

secondary chemistry was unimportant. However, using the directly measured^{35,36} $k_2 = 7.5 \times 10^{-11} \text{ cm}^3 \text{ s}^{-1}$, we conclude that their system should be described by the sequence of reactions



rather than simply H + O₂ + M. In the above mechanism, the first step is rate limiting, and the last is driven to completion by the large concentrations of H₂ in their system. Working backward, using presently known rates and branching fractions, we calculate that their observed rate, k_{obsd} , would have been

$$k_{\text{obsd}} = 2k_1(k_{2b} + k_{2c})/k_2 = 7 \times 10^{-33} \text{ cm}^6 \text{ molecule}^{-2} \text{ s}^{-1}$$

in good agreement with their results.

We feel that the results of Hikida, Eyre, and Dorfman³⁹ for M = Ar are compromised by secondary reactions of O atoms formed in the radiolysis pulse. For M = H₂ the reactions of excited O atoms with hydrogen should be rapidly driven to completion, but at the lower H₂ concentrations used in their M = Ar study these reactions could become comparable to the H + O₂ reaction. Similar problems with O atoms may underly the low and scattered values obtained in the two vacuum-UV flash photolysis studies.^{40,41}

The study of Cobos, Hippler, and Troe⁸ used laser photolysis of NH₃ at 193 nm to produce H atoms. Their NH₃/O₂/bath gas system was checked for ozone (and hence O atom) production with negative results. Their measured $k_{1,\text{Ar}} = (2.8 \pm 0.4) \times 10^{-32} \text{ cm}^6 \text{ s}^{-1}$ is in good agreement with this and other discharge-flow results, as is their rate $k_{1,\text{N}_2} = (6.5 \pm 1.0) \times 10^{-32} \text{ cm}^6 \text{ s}^{-1}$.

After critically surveying the literature, we find that, after applying the indicated corrections, seven of the reported rates for H + O₂ + (He, Ar) fall within common error bars. Averaging these rates, we suggest $k_{1(\text{He,Ar})} = (2.5 \pm 0.1) \times 10^{-32} \text{ cm}^6 \text{ s}^{-1}$ at 298 K. This rate is somewhat larger than those from CODATA and NASA^{6,7} evaluations, which were based on the flash photolysis results of Wong and Davis,⁴⁰ Kurylo,⁴¹ and Cobos et al.⁸ We likewise suggest values of $k_{1,\text{N}_2} = (6.3 \pm 0.7) \times 10^{-32} \text{ cm}^6 \text{ s}^{-1}$ and $k_{1,\text{H}_2\text{O}} = (6.3 \pm 0.8) \times 10^{-31} \text{ cm}^6 \text{ s}^{-1}$ at room temperature.

Troe has subjected the H + O₂ system to detailed theoretical study.^{8,42} With his formalism,¹⁶ the low-pressure recombination rate can be cast as

$$k_0 = \beta_c k^{\text{sc}}$$

where k^{sc} is the strong collision rate constant and β_c is the collision efficiency. β_c can be expressed in terms of the average energy, $\langle \Delta E \rangle$, transferred per collision between the AB intermediate and M:

$$\beta/(1 - \beta^{1/2}) = -\langle \Delta E \rangle / F_e k T$$

where F_e is a factor of order unity.¹⁶ k^{sc} is made up of two factors, a collision frequency, Z , and a factor, $k_{\text{AB}}^{\text{sc}}$, which can be calculated from properties of the two recombining species. Following Troe,¹⁶ we use Lennard-Jones collision rates

$$Z_{\text{LJ}} = \sigma^2 (8\pi k T / \mu)^{1/2} \Omega_{\text{LJ}}^{(2,2)*}$$

and calculate, using the data of Cobos et al.⁸ for H + O₂

$$k_{\text{AB}}^{\text{sc}} = 5.8 \times 10^{-22} \text{ cm}^3$$

This, coupled with our experimental rates and the appropriate Lennard-Jones collision frequencies,^{29,43} allow us to calculate $\beta_c(\text{He}) = 0.15$ and $\beta_c(\text{N}_2) = 0.34$.

However, for water this standard calculation yields a β_c greater

than 1, inconsistent with Troe's definition of β_c , which is constrained to be between 0 and 1.¹⁶ Initially, we chose to calculate the collision rate using the Stockmayer potential,^{29,44} which accounts for the additional dipole-dipole interaction between HO₂ and H₂O. The resulting expression for this collision rate is identical with that for the Lennard-Jones potential, except that the Lennard-Jones collision integral, $\Omega_{\text{LJ}}^{(2,2)*}$, is replaced by the analogous integral evaluated for the Stockmayer potential. Mason and Monchick have evaluated the collision integrals⁴⁴ and suggested appropriate combining rules.⁴⁵ At room temperature, this Stockmayer collision rate is about 25% larger than a Lennard-Jones rate, $Z_{\text{St}} = 4.9 \times 10^{-10} \text{ cm}^3/\text{s}$. Combining this with Troe's value for $k_{\text{AB}}^{\text{sc}}$ and our experimental rate gives $\beta_c = 2.6$ for M = H₂O.

In our search for a suitable collision rate, we next calculated a collisional capture rate,⁴⁶ analogous to the Langevin rate for ion-molecule reactions.⁴⁷ To do this, we considered only the dipole-dipole term in the Stockmayer potential. Following Johnston,⁴⁶ we calculated the capture collision rate for a given dipole-dipole orientation. This was then averaged over all attractive orientations, using Monte Carlo techniques. Experiments have shown that the effective dipole alignment is small in an ion-molecule collision;^{47,48} we therefore expect that the effective alignment during a dipole-dipole collision will be negligible and weigh each dipole-dipole orientation equally. The resulting collision rate is

$$Z_{\text{cc}} = 3.125(\mu_1\mu_2)^{2/3}(kT)^{-1/6}(m_{12})^{-1/2}$$

where μ_1 and μ_2 are the H₂O and HO₂ dipoles, and m_{12} is the reduced mass of the system. We calculated $Z_{\text{cc}} = 2.98 \times 10^{-10} \text{ cm}^3/\text{s}$, using $\mu_{\text{HO}_2} = 2.09 \text{ D}$.⁴⁹ This collision rate is even smaller than the Stockmayer rate and does not resolve our quandary.

A possible solution is to use total quantum mechanical scattering cross sections⁵⁰ for centrosymmetric r^{-6} or r^{-3} potentials. Using the Schiff-Landau-Lifshitz formulation, we can calculate the following collision rates⁵¹ and β_c 's:

$$\text{He:} \quad Z_{\text{SLL}} = 1.99 \times 10^{-9} \text{ cm}^3/\text{s}, \quad \beta_c = 0.022$$

$$\text{N}_2: \quad Z_{\text{SLL}} = 3.01 \times 10^{-9} \text{ cm}^3/\text{s}, \quad \beta_c = 0.034$$

$$\text{H}_2\text{O:} \quad Z_{\text{SLL}} = 5.1 \times 10^{-8} \text{ cm}^3/\text{s}, \quad \beta_c = 0.22$$

It is expected that this choice of collision frequency will also serve to explain the very large M effect for water observed in other systems, such as H + H + M ($k_{\text{H}_2\text{O}}/k_{\text{Ar}} \sim 10-20$)^{52,53} and H + OH + M ($k_{\text{H}_2\text{O}}/k_{\text{Ar}} \sim 20$).⁵³ We also hope that it will help us rationalize the temperature dependence we observed in the H + O₂ + M recombination.⁵⁴

Acknowledgment. We acknowledge the help of Dr. J. Jeffries, as well as discussions with Dr. J. Troe and Dr. M. F. Golde. We thank Dr. Stuart Anderson, whose careful reading of this manuscript was much appreciated. This work was supported by the ARO under Grant DAAG2985K0041.

Registry No. H, 12385-13-6; O₂, 7782-44-7; He, 7440-59-7; N₂, 7727-37-9; H₂O, 7732-18-5.

(44) Monchick, L.; Mason, E. A. *J. Chem. Phys.* **1961**, *35*, 1676.

(45) Mason, E. A.; Monchick, L. *J. Chem. Phys.* **1962**, *36*, 2746.

(46) Johnston, H. S. *Gas Phase Reaction Rate Theory*; Ronald: New York, 1966.

(47) Su, T.; Bowers, M. T. In *Gas Phase Ion Chemistry*, Vol. 1; Academic: New York, 1979; p 83.

(48) Bowers, M. T.; Laudenslager, J. B. *J. Chem. Phys.* **1972**, *56*, 4711.

(49) Saito, S.; Matsumura, C. *J. Mol. Spectrosc.* **1980**, *80*, 34.

(50) Pauly, H. *Atom Molecule Collision Theory*, Bernstein, R., Ed.; Plenum: New York, 1979; p 111.

(51) Durant, J. L.; Kaufman, F., manuscript in preparation.

(52) Homes, J. B.; Hurle, I. R. *Proc. R. Soc. London, Ser. A* **1970**, *A314*, 585.

(53) Getzinger, R. W.; Blair, L. S. *Combust. Flame* **1969**, *13*, 271.

(54) Hsu, K.-J.; Durant, J. L.; Anderson, S. M.; Kaufman, F., manuscript in preparation.

(55) Sridharan, U. C.; Qiu, L. X.; Kaufman, F. *J. Phys. Chem.* **1981**, *85*, 3361.

(56) Keyser, L. F. *J. Phys. Chem.* **1983**, *87*, 837.

(57) Zellner, R.; Steinert, W. *Chem. Phys. Lett.* **1981**, *81*, 568.

(58) Takas, G. A.; Howard, C. J. *J. Phys. Chem.* **1984**, *88*, 2110.

(39) Hikida, T.; Eyre, J. A.; Dorfman, L. M. *J. Chem. Phys.* **1971**, *54*, 3422.

(40) Wong, W.; Davis, D. D. *Int. J. Chem. Kinet.* **1974**, *6*, 401.

(41) Kurylo, M. J. *J. Phys. Chem.* **1974**, *76*, 3518.

(42) Cobos, C. J.; Troe, J. *J. Chem. Phys.* **1985**, *83*, 1010.

(43) Patrick, R.; Golden, D. M. *Int. J. Chem. Kinet.* **1983**, *15*, 1189.